NEUROSCIENCE

Best frequencies and temporal delays are similar across the low-frequency regions of the guinea pig cochlea

George Burwood[1], Pierre Hakizimana[2], Alfred L Nuttall[1]*, Anders Fridberger[1,2]*

The cochlea maps tones with different frequencies to distinct anatomical locations. For instance, a faint 5000-hertz tone produces brisk responses at a place approximately 8 millimeters into the 18-millimeter-long guinea pig cochlea, but little response elsewhere. This place code pervades the auditory pathways, where neurons have "best frequencies" determined by their connections to the sensory cells in the hearing organ. However, frequency selectivity in cochlear regions encoding low-frequency sounds has not been systematically studied. Here, we show that low-frequency hearing works according to a unique principle that does not involve a place code. Instead, sound-evoked responses and temporal delays are similar across the low-frequency regions of the cochlea. These findings are a break from theories considered proven for 100 years and have broad implications for understanding information processing in the brainstem and cortex and for optimizing the stimulus delivery in auditory implants.

INTRODUCTION

The auditory system consists of a set of "labeled lines" (*1*, *2*). Essentially, every neuron that exits the cochlea is assumed to have a distinct best frequency. When the pitch of a tone matches a neuron's best frequency, even a faint stimulus triggers a robust increase in the firing rate. It seems clear that the auditory system is organized in many parallel and relatively narrow channels, each responding best to a small range of stimulus frequencies.

Much of the data supporting this idea were generated using pure-tone stimuli, which contain only a single frequency. However, natural sounds are mixtures of different frequencies whose amplitudes change rapidly over time. When exposed to these sounds, auditory neurons from the brainstem to the cortex alter their response, sometimes in marked fashion (*3*, *4*).

These higher-order features may be a consequence of processing in the auditory brainstem nuclei and cortex. It is natural to think so because the organ of Corti is thought to map different stimulus frequencies to distinct places along the cochlear spiral (*5*, *6*). Each afferent neuron would therefore provide the brainstem with a measure of what is going on in the vicinity of one particular frequency, its best frequency.

However, is there really a unique best frequency for each cochlear location? Because of technical and anatomical constraints, little is known about the parts of the cochlea that encode sounds with frequencies of less than 1000 Hz. These low frequencies are important for speech perception, particularly for distinguishing vowels. It was only with the recent development of optical coherence tomography (OCT) vibrometry (Fig. 1A) (*7*–*9*) that it became possible to study these regions of the cochlea without the artifacts that plagued previous studies (*10*). However, an in-depth analysis of frequency specificity across the low-frequency regions is currently lacking.

Conventional theory makes explicit predictions. In Fig. 1B, the structural OCT image was color-coded according to the predicted best frequency of each place. The expectation is that the basal measurement site in Fig. 1A would respond best near 750 Hz, the middle location at 300 Hz, and the apical one at 90 Hz. Timing differences are also anticipated, with a 6-ms delay between the response of the basal and apical places (right color scale in Fig. 1B) (*11*).

Here, these predictions were systematically tested. We found no difference in the best frequency between the basal and middle measurement location in Fig. 1A, while the apical location had the highest best frequency. Response delays were either much smaller than expected or entirely absent. These features deviate completely from existing, widely accepted models (*6*, *12*, *13*). Apparently, places that are thousands of micrometers from each other have a similar response to sound, so the channels that pass information to the brainstem are wide, and the precise origin of nerve fibers within the low-frequency regions is not relevant. These findings have profound implications for understanding how communication-relevant sounds are processed and may also have clinical importance. By considering the distributed response made evident here, the stimulus delivered by auditory implants could be further optimized for improved speech and music recognition.

RESULTS

Studies reported here were performed in guinea pigs, a species whose low-frequency hearing is similar to the human one (*14*). To recover structural information and measure nanometer sound-evoked movements,

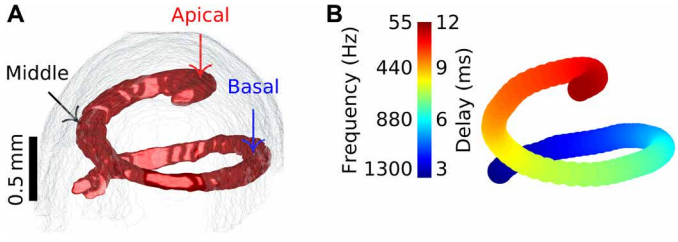

Fig. 1. Predicted response in the low-frequency regions of the cochlea. (**A**) OCT is an interferometric technique that uses infrared light to recover structural information and measure cell movements. Here, OCT data were used to reconstruct in three dimensions the outline of the organ of Corti (red) near the apex of the cochlea. The surrounding bone is light gray. Arrows point to the three measurement locations used in this study. (**B**) Using Greenwood's frequency-position function for the guinea pig (*6*), each place visible in the reconstruction in (A) was colored according to its expected best frequency (left scale). A corresponding gradient of response delays is also expected (right scale). The delays were derived from Siegel *et al.* (*11*).

[1]Oregon Hearing Research Center, Department of Otolaryngology–Head and Neck Surgery, Oregon Health & Science University, Portland, OR 97239, USA. [2]Department of Biomedical and Clinical Sciences, Linköping University, SE-581 83 Linköping, Sweden.
*Corresponding author. Email: nuttall@ohsu.edu (A.L.N.); anders.fridberger@liu.se (A.F.)

we guided the infrared light from a Thorlabs Telesto III OCT system toward the structures of interest by using a micromirror placed close to the apex of the cochlea. This arrangement obviates the need for a large opening in the bone surrounding the cochlea, so surgical trauma is reduced and the likelihood of recording from preparations in good physiological condition increases, compared to the surgical approach usually used when studying low-frequency hearing.

Sound-evoked responses are not consistent with accepted dogma

Figure 2A shows a morphological OCT scan. Superimposed on the grayscale structural image is the sound-evoked displacement at three locations along the hearing organ [the stimulus was a 200-Hz sine wave at 64 dB sound pressure level (dB SPL); color scale is displacement in nanometers]. The basal location had the largest response, followed by the middle and apical ones. The response of each site was determined at stimulus frequencies from 80 to 1000 Hz at levels between 44 and 64 dB SPL in 16 different animals.

When interpreting these data, spatial relations must be considered. Measurements on three-dimensional reconstructions (such as the one in Fig. 1A) revealed that the apical and basal sites in Fig. 2A were separated by 4300 μm along the coiled, 18-mm-long hearing organ; the apical site was located 360 μm from the helicotrema.

At 44 dB SPL, which is close to the guinea pig's hearing threshold at low frequencies, the peak response at the apical site was found at 315 Hz (Fig. 2B, red asterisks). There was no detectable response at less than 160 Hz. The middle and basal measurement locations behaved similarly, with maximal response at 80 Hz. At 64 dB SPL (right in Fig. 2B), the basal and middle sites had similar response again, with maximal magnitude at 160 Hz, but the apical site continued to respond best at 315 Hz. These results deviate completely from the predictions shown in Fig. 1B. To verify this finding, data were collected from 15 additional preparations.

Figure 2C shows the best-frequency differences across these 16 preparations, using the basal site as the reference. Differences predicted by the standard Greenwood model (*6*) are shown by the red and black target-like shapes. In contrast to predictions, note that the apical location (red asterisks in Fig. 2C) has higher best frequency than the basal one. Furthermore, there was no best-frequency difference between the basal and middle sites (black squares). These two places had similar best frequencies at all stimulus levels tested here.

Using a linear model fitted with generalized least squares (GLS), the most apical location was found to have significantly higher best frequency than the middle and basal location (P values ranging from 0.0001 to 0.004), but there was no significant difference in best

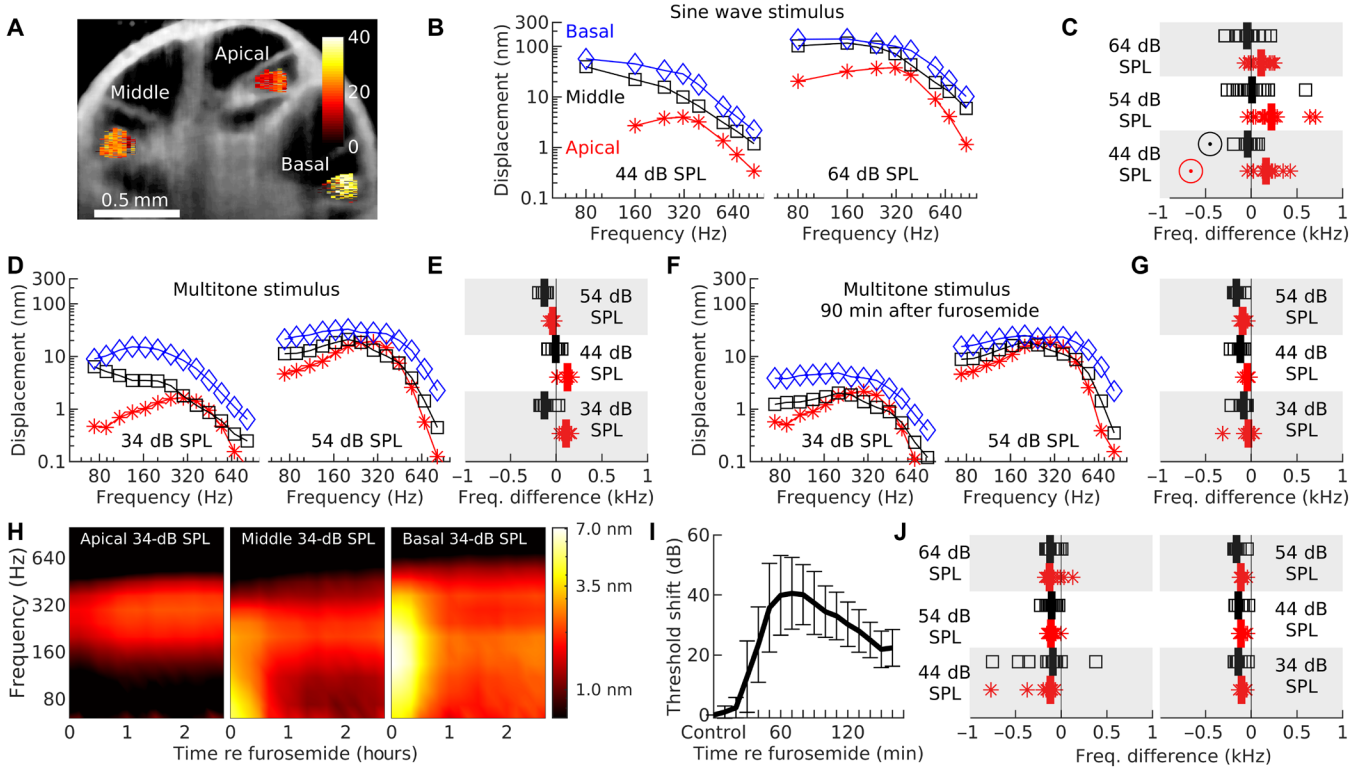

Fig. 2. Similar best frequencies across the low-frequency areas. (**A**) Morphological scan acquired by the OCT system (grayscale). Colored pixels show sound-evoked displacement amplitudes at 200 Hz and 64 dB SPL (color map in nanometers). (**B**) Response amplitudes at the locations in (A). (**C**) Best-frequency differences measured with pure tones. The red color shows data from the apical site; the black color denotes the middle site. The "target" shapes show the difference predicted by standard theory. Black and red bars show medians. (**D**) Response to tone complexes with 15 components. Colors and symbols as in (B). (**E**) Best-frequency differences across eight preparations using the multitone stimulus. Conventions as in (C). (**F**) Response amplitudes 90 min after furosemide. (**G**) Best-frequency differences of the same group as in (E), 90 min after furosemide. Conventions as in (C) and (E). (**H**) Mean displacement after furosemide ($n = 7$; 34 dB SPL). Color scale gives displacement magnitude. (**I**) Mean threshold shift in round window compound action potential evoked by a 2-kHz tone demonstrates the global decrease in cochlear function induced by furosemide. (**J**) Postmortem best-frequency differences for sine (left; $n = 16$) and multitone stimulation (right; $n = 8$). Recordings started 30 min after the death of the animal.

frequency between the basal and middle location at any stimulus level (P values between 0.2 and 0.87; detailed statistical information is given in table S1). Apparently, the response to pure tones at stimulus levels between 44 and 64 dB SPL is similar across a large portion of the organ of Corti near the apex. The difference that is present is in the opposite direction from the prediction illustrated in Fig. 1B.

We were concerned about two possible problems. First, data collection is time-consuming when pure-tone stimuli are used, raising the possibility that sample drift or physiological changes could influence results. Second, pure tones are not a natural stimulus. To remedy both problems, experiments were performed using tone complexes, which allow a dataset to be acquired in less than 5 min. Fifteen different frequencies were included in the stimulus, which was delivered at stimulus levels per frequency between 34 and 54 dB SPL (calibrations performed in each animal ensured an identical stimulus level across all frequencies; in subsequent graphs, we plot the amplitude and phase for each frequency component). These tone complexes are likely to enhance nonlinearity below the best frequency (*15*). To compensate for this effect, multitone stimuli were applied at lower stimulus level than the pure tones.

The use of a more natural stimulus changed the hearing organ's response (left in Fig. 2D). Instead of the low-pass shape seen in Fig. 2B, the basal and apical sites showed more pronounced peaks. When the stimulus level increased to 54 dB SPL, curves from all three sites were similar, with nearly identical best frequencies and amplitudes (right in Fig. 2D).

Figure 2E summarizes results from eight different preparations. The apical site had significantly higher best frequency at both 34 and 44 dB SPL ($P = 7 \times 10^{-4}$ and $P = 2.2 \times 10^{-5}$; table S2). The middle site was tuned to a lower frequency than the basal site at both 34 and 54 dB SPL ($P = 0.001$ and $P = 1.1 \times 10^{-11}$), but there was no difference at 44 dB SPL ($P = 0.44$). Thus, while some numerical differences were present, the shape of the curves was so similar that these differences are unlikely to have physiological importance. The response was effectively the same throughout the apex when a multitone stimulus was used.

In summary, Fig. 2 (A to E) shows that there was no difference in best frequency between the basal and middle sites when pure tones were used. With multitone stimuli, these two places had the same best frequency at 44 dB SPL, while a small difference was present at 34 and 54 dB SPL. These properties, and the consistently higher best frequency for the apical site, are far from predictions, which suggest a monotonic best-frequency gradient of −3.1 octaves between the basal and apical measurement sites. With sine wave stimuli, the measured gradients between the basal and apical sites were +0.8, +0.94, and +0.45 octaves at 44, 54, and 64 dB SPL, illustrating the considerable difference between the theoretical map (Fig. 1B) and the one measured here.

Outer hair cells actively distribute excitation to new places

To determine whether the sound-evoked response depended on force produced by outer hair cells (*16*, *17*), sound-evoked responses were examined after intraperitoneal administration of furosemide (100 mg/kg of body weight), a diuretic known to abolish the positive electrical potential that normally is present near the hearing organ (*18*). When this standing potential declines, the electrical gradient across mechanically sensitive ion channels decreases, causing smaller receptor potentials and reduced force production from outer hair cells (*19*).

At 34 dB SPL, furosemide reduced the response at the basal and middle site, and their peak response shifted to higher frequencies (Fig. 2F, left; data are from the same preparation as in Fig. 2D). At the apical site, the sound-evoked response paradoxically increased, while the best frequency remained stable near 300 Hz. At 54 dB SPL, curves from the three locations were very similar. The differences between sites were too small to be functionally important.

The minor frequency differences in Fig. 2F are reflected in the summary statistics (Fig. 2G). At 34 dB SPL, furosemide moved the best frequency of the basal location to higher values. As a result, the basal and apical locations shared the same best frequency ($P = 0.34$; table S3). A similar result was evident at 44 dB SPL ($P = 0.12$), but at the highest stimulus level, the apical site had significantly lower best frequency than the basal site ($P = 2.1 \times 10^{-9}$). The middle site had the lowest best frequency throughout (P values of 0.0007, 5.6×10^{-5}, and 2.7×10^{-20}). The results in Fig. 2G show that the outer hair cells expand the response area of the hearing organ by moving the best frequency of the basal and middle sites to lower frequencies.

To show how the furosemide-induced changes developed, color-coded data are displayed in Fig. 2H (means, $n = 7$). The influence of furosemide was evident after 30 min and plateaued at 1.5 hours. At this point in time, a large decrease in response magnitudes was evident for the basal and middle sites. This reduction was pronounced at low stimulus frequencies and caused the best frequency to shift upward. The best frequency was stable at the apical site, where response magnitudes generally increased.

Changes induced by furosemide were reflected in neural thresholds. The threshold for the compound action potential of the auditory nerve worsened by close to 40 dB after 80 min (Fig. 2I; note that compound action potentials cannot be reliably recorded at low frequencies, so this figure reports data at a stimulus frequency of 2 kHz), which is consistent with the mechanical data in Fig. 2H.

Outer hair cells stop producing force after the death of the animal. Postmortem measurements can therefore be used to assess the influence of outer hair cell activity on sound-evoked responses. A remarkable change occurred postmortem, with the best frequency of the basal and middle sites increasing by more than one octave after the animal died (with 44 dB SPL of sine wave stimulation, the basal best frequency changed from 240 ± 70 to 610 ± 200 Hz postmortem, middle location from 200 ± 70 to 460 ± 160 Hz; apical location from 400 ± 130 to 430 ± 50 Hz). The change for the apical location was not statistically significant ($P = 0.59$), but changes for the other two locations were statistically significant (middle: $P = 1.1 \times 10^{-5}$; basal: $p = 2.4 \times 10^{-6}$; table S4). As evident from Fig. 2J, there was no best-frequency difference between the postmortem apical and middle locations regardless of the type of stimulus used.

In summary, Fig. 2 shows that differences in best frequency across the apical regions of the cochlea are too small to be functionally relevant. Furthermore, rather than concentrating sound-evoked responses on a small region, as is the case in high-frequency cochlear regions, the motor activity of the outer hair cells distributes the response to larger numbers of sensory cells. This is a stark departure from widely accepted theories.

Minimal delay between sensory cells provides a substrate for signal processing

The distribution of the sound-evoked response across a long region of the organ of Corti evident in Fig. 2 suggests that low-frequency

hearing could benefit from averaging or correlating neuronal responses across many cells. For this to work optimally, the time delay between different cochlear locations should be minimized. Information about these delays can be derived from the local slope of phase-frequency curves.

The slopes of the phase curves for the middle and the basal location were similar throughout the frequency range (Fig. 3A, left, 34 dB SPL), suggesting that these locations respond with similar delay to the acoustic stimulus. For frequencies less than 160 Hz, the phase slope at the apical location was close to the other locations, but the slope thereafter increased with frequency, indicating a gradually increasing travel time. At 54 dB SPL (Fig. 3A, right), the phase curves changed, and the slopes for the middle and apical locations became slightly larger than the basal location, indicating the emergence of travel time differences.

Ninety minutes after furosemide (Fig. 3B), the phase curves at 34 dB SPL were close to the ones recorded at 54 dB SPL before furosemide, indicating that force produced by outer hair cells affected the response delay. The phase-frequency curves never became linear, indicating that the propagation delay always depends on the stimulus frequency. In systems with frequency-dependent delays, response delays are usually quantified as the group delay, because computations based on raw phase values are unreliable (*20*).

For the basal location, the group delay decreased with frequency at a rate of −2.8 μs/Hz ($r^2 = 0.66$; $P < 2 \times 10^{-16}$; 34 dB SPL; table S5). To show how the delay varied between locations, Fig. 3C displays the difference in group delay relative to the basal site. For frequencies less than 400 Hz, there was no average delay between the middle and the basal location. A small delay appeared at higher frequencies, but the delay decreased again at frequencies higher than 600 Hz. After intraperitoneal furosemide, the delay difference to the basal location increased significantly ($P = 1.25 \times 10^{-12}$ for the comparison between delays before and 90 min after furosemide; n = 7; Fig. 3D and table S6).

The apical location behaved differently. At low stimulus frequencies, it had shorter delay than the other two sites (Fig. 3, C and D, red dots and curve). The delay difference increased with frequency to reach a peak around 400 Hz and then again turned negative

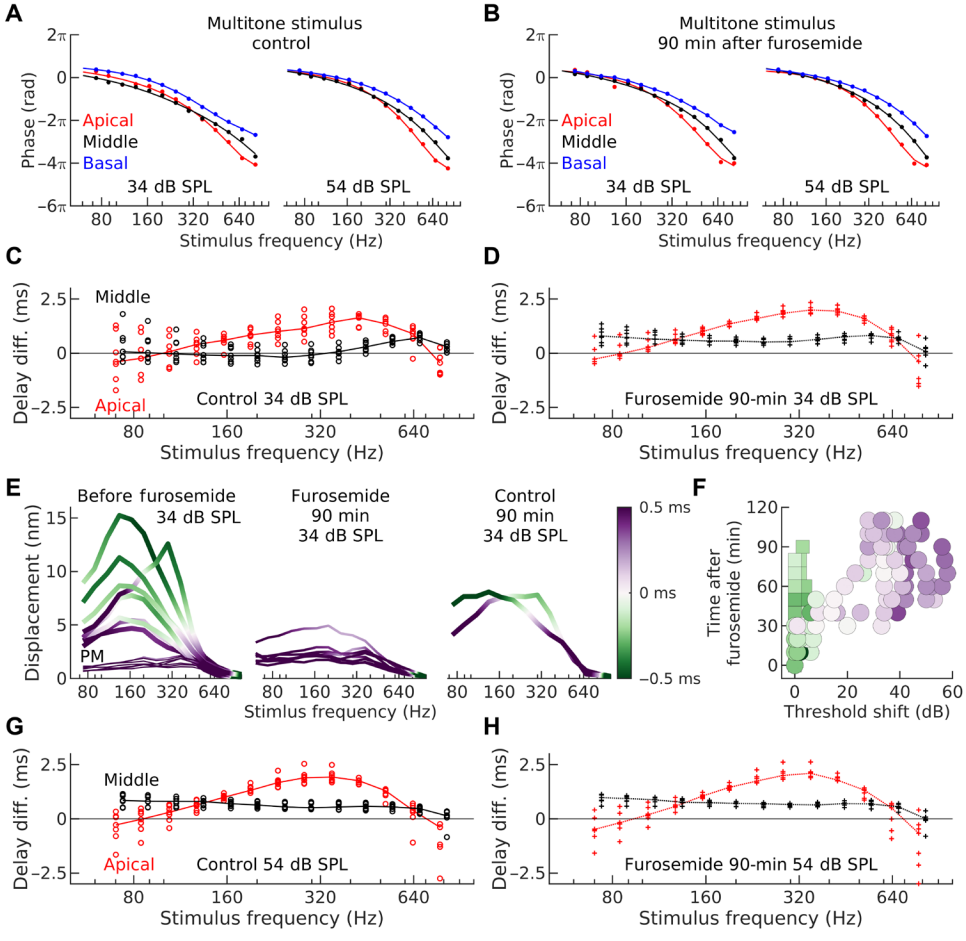

Fig. 3. Outer hair cell activity minimizes response delays. (**A** and **B**) Phase curves in the same preparation before (A) and after (B) furosemide. Dots show measured values, and solid lines are fits to fourth-order polynomial functions. (**C** and **D**) Differences in group delay between the three sites, using the basal place as the reference. Solid lines are medians (n = 8). (**E**) Response amplitudes at the basal location before furosemide (n = 8; left), postmortem (PM; n = 8; left), after furosemide (n = 8; middle), and in two control preparations (right). Colors correspond to delays between the basal and the middle location (color scale on the right). (**F**) Compound action potential threshold shift after furosemide is correlated to the response delay. Color scale as in (E). Squares denote control preparations; circles are animals given furosemide. (**G** and **H**) Group delay differences at 54 dB SPL before (G) and after (H) furosemide (n = 8).

above 700 Hz. Although a tendency to increasing delay was present at low frequencies after furosemide (Fig. 3D), this was not statistically significant ($P = 0.12$).

The group delay showed considerable variability across preparations at 34 dB SPL (Fig. 3C). This capriciousness became smaller after furosemide (Fig. 3D), suggesting that variability may be related to outer hair cell force generation. To evaluate this possibility, Fig. 3E shows data from the basal location in seven different preparations. Each curve was colored according to the difference in delay between the basal and the middle location. Note that large magnitudes were consistently associated with negative delays near the peak. Hence, much of the variation seen in Fig. 3C is related to minor differences in hearing sensitivity among preparations.

To verify this result, we examined postmortem data (Fig. 3E, left, curves labeled PM). In these recordings, delays were always positive. A similar pattern was evident after furosemide (Fig. 3E, center). Data from two control preparations (where sound-evoked responses were tracked over time without any furosemide injection) were consistent with these results (Fig. 3E, right). Delays also correlated with the threshold of the auditory nerve compound action potential (Fig. 3F). At zero threshold, shift delays were negative (circles, squares show data from two control preparations, and color scale is the same as in Fig. 3E), but as the threshold shifts accumulated, delays increasingly turned positive.

At higher stimulus levels (54 dB SPL; Fig. 3G), the delay between the basal and middle location was positive and nearly constant across frequency, a pattern that persisted after furosemide (Fig. 3H). The most apical location had shorter delays than the middle one at very low and very high frequencies, both before and after furosemide [red dots and lines in Fig. 3 (G and H)].

Data acquired during sine wave stimulation had higher noise levels than the multitone data, but findings were similar. At low frequencies (80, 160, and 240 Hz), the median delay between the basal and the middle site was negative (−30, −370, and −150 μs, respectively; 44 dB SPL; 16 preparations). At stimulus frequencies between 320 and 860 Hz, the delays between these two sites were positive, while negative values were observed near 1 kHz.

The above data indicate that the motor activity of the outer hair cells minimizes the response delay between different apical locations. At low stimulus levels, a large section of the cochlear apex has the same delay. These findings are not consistent with predicted delays (Fig. 1B) and not with a traveling wave as commonly construed.

Features of these responses can be reproduced with other measurement techniques

The above findings represent a fundamental departure from standard theories, so we found confirmation with a different measurement technique to be essential. While no technique other than OCT can measure the response of a fully intact cochlea in vivo, some aspects can be confirmed using laser interferometry on isolated preparations (*8*). These in vitro preparations do not fully retain the active mechanisms that dominate the in vivo response at low stimulus levels, but basic aspects of sensory transduction are intact and functioning.

In the isolated preparation, sound-evoked responses were measured from two sites within the apical turn, with an average separation of 1.3 ± 0.3 mm ($n = 11$; the two measurement sites are marked by blue and red asterisks in Fig. 4A). By applying a similar logarithmically spaced tone complex as in Figs. 2 and 3, we found that the apical site had a smaller response, a difference that was consistently found (73 dB SPL: $P = 5.7 \times 10^{-7}$; Fig. 4B and table S7). This confirms the data in Fig. 2 (C and E), where a smaller response is seen for the most apical site.

Despite the similar shape of the curves (Fig. 4B), there was a minor difference in best frequency (basal site, 205 ± 40 Hz; apical site, 213 ± 37 Hz; $P = 4.7 \times 10^{-4}$; table S8). The higher best frequency for the apical location is consistent with the data in the right panel of Fig. 2J.

Visually, data acquired in vitro had sharper peaks than the ones acquired in vivo. This effect arises in part because laser interferometric measurements require the cochlear bone to be opened, which reduces the response at very low stimulus frequencies (*21*). Because the high-frequency part of the response is unaffected, a linear fit on this part of the curve was used to determine the slope. While the variance was considerable (Fig. 4C), the average slope was larger in vitro (−0.12 ± 0.08 nm/Hz versus −0.02 ± 0.016 nm/Hz; $P = 1.6 \times 10^{-8}$; table S9), suggesting that the apex of a fully active cochlea has an expanded frequency response. This is consistent with Fig. 2H, where furosemide "contracted" the frequency response at both the middle and the basal site.

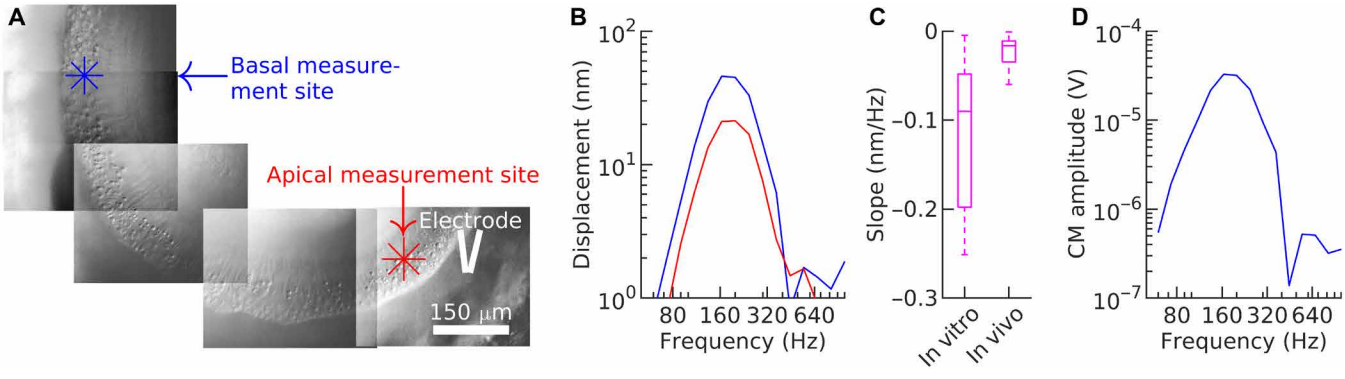

Fig. 4. Laser interferometry confirms essential aspects of in vivo data. (**A**) Images acquired using a digital camera were mounted to show the places where sound-evoked displacements were measured. In this experiment, a recording electrode was placed near the apical measurement site. (**B**) Response amplitudes at 73 dB SPL per frequency point at a basal (blue) and apical (red) measurement location. (**C**) Tuning curve slopes measured by a linear fit on data points to the right of the peak, excluding points near the noise floor (in vitro, $n = 11$; in vivo, $n = 8$). (**D**) Amplitude of the cochlear microphonic potential (CM) measured by the electrode in scala media. Stimulus level, 73 dB SPL.

In the experiment shown in Fig. 4A, a beveled glass microelectrode with 5-megohm resistance was placed near the sensory cells. This electrode was used to measure sound-evoked electrical responses (Fig. 4D), which were found to resemble the mechanical tuning curves. Because these potentials depend on mechanically sensitive ion channels being intact, this shows that a basic aspect of hearing organ physiology was functioning in these preparations. In summary, important aspects of the OCT data, such as lower response amplitudes and higher best frequency for the most apical location, were confirmed when using a different measurement technique in isolated preparations of the temporal bone.

DISCUSSION

Here, we demonstrated that low-frequency hearing works according to a unique principle that does not involve a place code. Instead, the sensory outer hair cells actively distribute sound-evoked responses across a long segment of the hearing organ, which responds with little interlocation delay. These findings, which are illustrated in Fig. 5 for a low-level pure-tone stimulus at 300 Hz, deviate radically from the standard, widely accepted theory (Fig. 1B). The difference is important because speech sounds, particularly vowels, contain much information at frequencies of less than 1 kHz. Low frequencies are also important for music perception, which is evident from the fact that the left half of a piano keyboard produces tones with fundamental frequencies of less than 1 kHz.

The lack of a place code means that low-frequency pitch perception must rely on the timing of action potentials in the auditory nerve, as suggested by psychophysical studies (*22*). A different mechanism seems to operate at high frequencies (*23*–*25*), a finding that is consistent with single-fiber responses recorded from the auditory nerve. When comparing fibers with low and high best frequencies, there are differences in response polarity (*26*–*28*), sharpness of tuning (*29*), and tuning curve shape. Bandpass tuning appears to be most common in low-frequency auditory nerve fibers (*30*–*32*), but complex tuning curves with multiple peaks are also reported [(*33*); figure 3A in (*34*)]. The discrepancy between the mechanical tuning curves shown here and published auditory nerve tuning curves suggest that processing of signals occur within the organ of Corti. Possible mechanisms include a presumed velocity dependence of inner hair cell stereocilia deflections [(*35*); however, see also (*36*, *37*)] or a filtering effect stemming from adaptation of mechanoelectrical transducer currents (*38*).

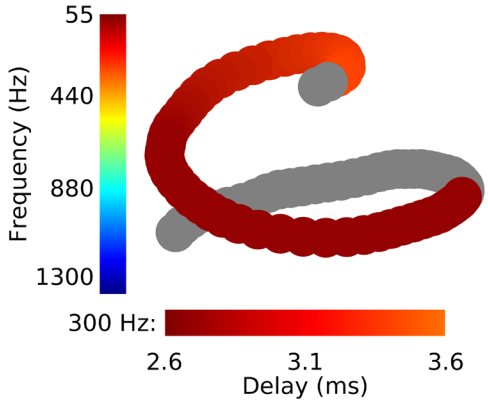

Fig. 5. Best frequencies and response delays are similar throughout the low-frequency region. Here, the best frequency was color-coded to show the similarity of best frequencies across much of the apex and the higher best frequency for the most apical location. To facilitate comparison with the Greenwood model, the frequency color scale on the left is identical to the one in Fig. 1B. Using the phase data shown in Fig. 3, we computed absolute delays (in milliseconds; horizontal color scale) at 34 dB SPL and 300 Hz. At this frequency, the most apical location has slightly longer delay than the basal and middle location; this is, however, not the case at all frequencies. Note the difference with the conventional theory (Fig. 1B).

The present findings mean that a large number of low-frequency nerve fibers must share a similar response. This could make it possible for the brain to average or correlate the sound-evoked response across nerve fibers, which would have advantages for signal detection and system robustness. The similarity of response delays across the apex of the cochlea would facilitate this signal processing (Fig. 3 and see also the summary in Fig. 5).

These results have implications for information processing in auditory implants, devices that restore hearing via electrical stimulation of neurons. Many implants use the classical theory (Fig. 1B) to map different stimulus frequencies to different electrodes. Notably, patients show superior low-frequency pitch discrimination if their implant provides temporal information [(*39*), figure 2)], and a pitch-matching study on a cochlear implant recipient with good contralateral hearing suggested that the place of apical electrodes did not affect the perceived pitch (*40*). Given the present results, it does not seem unexpected that devices providing phase-locked stimulation to the apex perform better, because the normal cochlear apex lacks a mechanical place code.

In conclusion, sensitive low-frequency hearing relies on the sensory outer hair cells to actively distribute sound-evoked responses across large segments of the hearing organ while minimizing propagation delays. Given the capacity for inner hair cells and auditory nerve fibers to phase lock to the stimulus (*41*) and the potential for multiple inner hair cells to be electrically coupled (*42*), we propose that averaging of sound-evoked responses across populations of neurons underlies our ability to distinguish the pitch of low-frequency sounds.

MATERIALS AND METHODS

Surgical preparation

Data from 37 albino guinea pigs of both sexes and weighing less than 400 g are included in this study. Sixteen animals were used for single-tone experiments and 10 for multitone experiments. Eleven were used for in vitro experiments. All in vivo procedures were conducted with permission of the institutional animal care and use committee at Oregon Health & Science University (permit IP00001278). In vitro experiments were approved by the Regional Ethics Committee in Linköping, Sweden (permit 5111/2019).

The in vivo experiments were performed inside a double-walled sound attenuation booth with the preparation housed on a vibration-isolation table. Minimally invasive surgical procedures were used to get access to the cochlear apex. Briefly, guinea pigs were anesthetized using intramuscular injections of ketamine (40 mg/kg of body weight) and xylazine (10 mg/kg). Supplemental anesthesia was administered at 50% of the initial dose every hour. Local analgesics (lidocaine, 1 mg/ml) were injected subcutaneously on the head and throat, and areflexia was checked via toe pinch.

After anesthesia, the pinna was resected, the animal was tracheostomized, and the skull was fixed in a custom head holder. The auditory bulla was exposed and gently opened under a dissection microscope, using a scalpel blade. A Teflon-coated silver-silver chloride electrode wire with a ball point was placed in the round window niche and cemented to the bulla. A reference electrode was then secured in the neck muscles, and a closed-field, calibrated sound system consisting of two speakers and a microphone was coupled into the ear canal. Initial cochlear sensitivity was appraised using measurements of compound action potential thresholds. Sinusoidal stimuli shaped using a raised cosine were manually deattenuated until the synchronized action potential response could be seen on an oscilloscope screen. The attenuation was then increased until the action potential disappeared. Sensitivity was checked for a frequency range of 2 to 36 kHz. Compound action potentials were checked regularly during the experiment and before administration of furosemide. Data from animals with more than 10-dB change in compound action potential thresholds at 2 and 4 kHz were discarded.

While widening the opening in the auditory bulla, the amplitude of the 900-Hz electrical distortion product evoked by a pair of tones at 18 and 18.9 kHz was continuously monitored using the electrode in the round window niche. Whenever the amplitude of the 900-Hz distortion product decreased, dissection was temporarily halted until the peak amplitude returned. In all experiments, the tensor tympani muscle was sectioned.

To permit vibration measurements without extensive dissection, a glass coverslip measuring approximately 2 mm^2, sputter-coated with gold, was placed in the bulla, close to the apex. The cover slip reflected the infrared light of the OCT system to the apex. The animal was wrapped in a heating blanket throughout the experiment, and its temperature was measured with a rectal thermometer.

Optical coherence tomography

OCT measurements were made using a Thorlabs Telesto III system with a central wavelength of 1300 nm. Custom LabVIEW software was used for acquisition and sound calibration. The scan head of the OCT machine was placed over the preparation and was focused using a camera integrated with the OCT system. The cochlea was imaged with a ×5 objective lens with a numerical aperture of 0.44. Care was taken to measure from similar angles in all preparations. A single unaveraged vibrometry scan was made to acquire the organ of Corti sections, and small regions of interest were selected to avoid scanning nonrelevant structures. Calibrated sinusoidal and complex stimuli were used to evoke organ of Corti vibrations, which were then sampled at 10 kHz by the custom LabVIEW software. The sound pressure level was controlled using a programmable attenuator. Recordings were made before and after furosemide administration, and at least 30 min postmortem. Reference recordings were made from the head of the stapes postmortem.

Acoustic stimuli

Sinusoidal tones between 80 and 1000 Hz were used. Complex stimuli consisted of 15 approximately logarithmically spaced tones between 72 and 1000 Hz. Each component had a random phase and an integer number of samples within the acquisition window (the frequencies present in the tone complex were rounded to the nearest multiple of 1 Hz to ensure this; the stimulus duration was 1 s). In each experiment, an in situ calibration of sound pressures was performed to ensure that the stimulus had the same sound pressure level at all frequencies. Only complex stimuli were used for furosemide experiments.

Furosemide experiments

Baseline vibration scans were made in response to complex stimuli at 34, 44, and 54 dB SPL per frequency point. Compound action potential tuning curves were then recorded, and the threshold at 2 kHz was noted. Furosemide (100 mg/kg) was injected through an intraperitoneal cannula. A subsequent set of level functions were taken immediately after injection and every 10 min hence. Compound action potentials (2 kHz) were monitored, and the experiment was ended when a plateau in the recovery was seen (usually at around 2.5 hours). In control preparations, the sound-evoked response was tracked over the same time frame, but without injecting furosemide. The sound system was recalibrated every 30 min.

In vitro experiments

Young guinea pigs weighing less than 400 g were deeply anesthetized with intraperitoneal sodium pentobarbital and were decapitated. The temporal bone was excised, and the auditory bulla was carefully opened after attaching the preparation to a plastic holder, with the ear canal facing a calibrated loudspeaker. A small opening was made in scala tympani at the base of the cochlea. This opening was used to perfuse the cochlea with oxygenated tissue culture medium. The perfusion medium exited the cochlea through a second opening in scala vestibuli in the apical turn. Because the present experiments recorded vibrations from widely separated sites within the apical turn, this apical opening was deliberately made larger than the opening used in previous studies [e.g., (*37*)]. The large opening results in a loss of effective stimulation at low frequencies (*21*). The tuning curves measured from the preparation are therefore sharper than those that would be recorded from a closed cochlea. The immersion of the preparation in tissue culture medium reduces the effective stimulus level by about 20 dB. Sound pressure levels given in the text were corrected for this effect.

Sound-evoked displacements were measured from the preparations using confocal laser interferometry (*8*). In each experiment, a glass microelectrode with 5- to 8-megohm impedance was placed inside scala media. The electrode was used to measure sound-evoked electrical potentials.

Data analysis

Vibration data were analyzed using custom MATLAB software, using the approach described in (*43*) to recover the displacement at each stimulus frequency. This was done by two successive fast Fourier transforms. The amplitude of the first transform gives the morphological image (Fig. 2A). The phase data are used to compute the cellular motion through a second fast Fourier transform. Using morphological OCT images, regions of interest were drawn around the organ of Corti corresponding to the three locations described in the text (apical, middle, and basal). The region of interest included all the organ of Corti except the basilar membrane. The region with the highest optical reflectivity is usually found near the third row of outer hair cells, so the response of this region dominates our recordings, just like it does in previous studies (*9*). Within each region of interest, pixels where the sound-evoked displacement had signal-to-noise ratio better than 6 dB were averaged, and the magnitude and phase were extracted. Phase was corrected for the middle

ear phase response measured at the stapes, but the amplitude data were not corrected. Data are presented as means or medians with SD. Because many of the tuning curves had low-pass characteristics, the best frequency was defined as the frequency at which the amplitude of the isoresponse tuning curve had declined by 3 dB from the peak value.

Phase-frequency curves such as the ones shown in Fig. 3A were used to calculate group delays. The group delay is measured in seconds and is defined as the negative of the local phase slope divided by 2π (*20*). To measure the slope, the unwrapped phase-frequency curves were fitted with a fourth-order polynomial and the derivative at each frequency determined from the fitted polynomial. Fits were generally excellent with small residuals. Alternative methods for determining the derivative, such as simple or central differences, were used initially, but these methods were associated with higher noise levels and also forced data points at the beginning of the phase-frequency curve to be discarded.

Statistics

Magnitude and phase curves are acquired by measuring the response of each preparation while presenting stimuli at different frequencies and levels. This process of repeated measurements introduces correlations within the data. To account for these correlations, linear models were fitted with GLS using the gls function in the nlme package of R (release 3.6.0 running on Centos 7.9). When evaluating differences in best frequencies between the basal, middle, and apical sites, the measurement site was treated as the independent variable, and correlations within the dataset assumed to be uniform in each individual preparation.

SUPPLEMENTARY MATERIALS

Supplementary material for this article is available at https://science.org/doi/10.1126/sciadv.abq2773

View/request a protocol for this paper from *Bio-protocol*.

REFERENCES AND NOTES

1. E. R. Kandel, J. H. Schwartz, T. M. Jessel, Eds., Hearing, in *Principles of Neural Science* (McGraw-Hill, ed. 4, 2000), pp. 590–613.
2. K. Jasmin, C. F. Lima, S. K. Scott, Understanding rostral–caudal auditory cortex contributions to auditory perception. *Nat. Rev. Neurosci.* **20**, 425–434 (2019).
3. A. Mizrahi, A. Shalev, I. Nelken, Single neuron and population coding of natural sounds in auditory cortex. *Curr. Op. Neurobiol.* **24**, 103–110 (2014).
4. N. C. Rabinowitz, B. D. B. Willmore, A. J. King, J. W. H. Schnupp, Constructing noise-invariant representations of sound in the auditory pathway. *PLOS Biol.*. **11**, e1001710 (2013).
5. G. von Békésy, *Experiments in Hearing* (McGraw-Hill, 1960).
6. D. D. Greenwood, A cochlear frequency-position function for several species–29 years later. *J. Acoust. Soc. Am.* **87**, 2592–2605 (1990).
7. F. Chen, D. Zha, A. Fridberger, J. Zheng, N. Choudhury, S. L. Jacques, R. K. Wang, X. Shi, A. L. Nuttall, A differentially amplified motion in the ear for near-threshold sound detection. *Nat. Neurosci.* **14**, 770–774 (2011).
8. R. L. Warren, S. Ramamoorthy, N. Ciganovic, Y. Zhang, T. M. Wilson, T. Petrie, R. K. Wang, S. L. Jacques, T. Reichenbach, A. L. Nuttall, A. Fridberger, Minimal basilar membrane motion in low-frequency hearing. *Proc. Natl. Acad. Sci. U.S.A.* **113**, E4304–E4310 (2016).
9. A. Recio-Spinoso, J. S. Oghalai, Mechanical tuning and amplification within the apex of the guinea pig cochlea. *J. Physiol.* **595**, 4549–4561 (2017).
10. N. P. Cooper, W. S. Rhode, Fast travelling waves, slow travelling waves and their interactions in experimental studies of apical cochlear mechanics. *Aud. Neurosci.* **2**, 289–299 (1996).
11. J. H. Siegel, A. J. Cerka, A. Recio-Spinoso, A. N. Temchin, P. van Dijk, M. A. Ruggero, Delays of stimulus-frequency otoacoustic emissions and cochlear vibrations contradict the theory of coherent reflection filtering. *J. Acoust. Soc. Am.* **118**, 2434–2443 (2005).
12. J. Tsuji, M. C. Liberman, Intracellular labeling of auditory nerve fibers in guinea pig: Central and peripheral projections. *J. Comp. Neurol.* **381**, 188–202 (1997).
13. A. Viberg, B. Canlon, The guide to plotting a cochleogram. *Hearing Res.* **197**, 1–10 (2004).
14. R. Heffner, H. Heffner, B. Masterton, Behavioral measurements of absolute and frequency-difference thresholds in guinea pig. *J. Acoust. Soc. Am.* **49**, 1888–1895 (1970).
15. E. Fallah, C. E. Strimbu, E. S. Olson, Nonlinearity and amplification in cochlear responses to single and multi-tone stimuli. *Hearing Res.* **377**, 271–281 (2019).
16. W. E. Brownell, C. R. Bader, D. Bertrand, Y. de Ribaupierre, Evoked mechanical responses of isolated cochlear outer hair cells. *Science* **227**, 194–196 (1985).
17. A. Vavakou, N. P. Cooper, M. van der Heijden, The frequency limit of outer hair cell motility measured in vivo. *eLife* **8**, e47667 (2019).
18. C. E. Strimbu, Y. Wang, E. S. Olson, Manipulation of the endocochlear potential reveals two distinct types of cochlear nonlinearity. *Biophys. J.* **119**, 2087–2101 (2020).
19. M. A. Ruggero, N. C. Rich, Furosemide alters organ of corti mechanics: Evidence for feedback of outer hair cells upon the basilar membrane. *J. Neurosci.* **11**, 1057–1067 (1991).
20. A. V. Oppenheimer, R. W. Schafer, J. R. Buck, Transform analysis of linear time-invariant systems, in *Discrete-Time Signal Processing* (Prentice-Hall, ed. 2, 1999), pp. 242–243.
21. M. Ulfendahl, S. B. M. Khanna, A. Fridberger, Å. Flock, B. Flock, W. Jäger, Mechanical response characteristics of the hearing organ in the low-frequency regions of the cochlea. *J. Neurophysiol.* **76**, 3850–3862 (1996).
22. B. C. J. Moore, Frequency difference limens for short-duration tones. *J. Acoust. Soc. Am.* **54**, 610–619 (1973).
23. B. K. Lau, A. H. Mehta, A. J. Oxenham, Superoptimal perceptual integration suggests a place-based representation of pitch at high frequencies. *J. Neurosci.* **37**, 9013–9021 (2017).
24. J. O. Pickles, Auditory pathways: Anatomy and physiology. *Handb. Clin. Neurol.* **129**, 3–25 (2015).
25. E. Verschooten, S. Shamma, A. J. Oxenham, B. C. Moore, P. X. Joris, M. G. Heinz, C. J. Plack, The upper frequency limit for the use of phase locking to code temporal fine structure in humans: A compilation of viewpoints. *Hear. Res.* **377**, 109–121 (2019).
26. T. Konishi, D. W. Nielsen, The temporal relationship between basilar membrane motion and nerve impulse initiation in auditory nerve fibers of guinea pigs. *Jpn. J. Physiol.* **28**, 291–307 (1978).
27. W. G. Sokolich, R. P. Hamernik, J. J. Zwislocki, R. A. Schmiedt, Inferred response polarities of cochlear hair cells. *J. Acoust. Soc. Am.* **59**, 963–974 (1976).
28. A. N. Temchin, A. Recio-Spinoso, H. Cai, M. A. Ruggero, Traveling waves on the organ of Corti of the chinchilla cochlea: Spatial trajectories of inner hair cell depolarization inferred from responses of auditory-nerve fibers. *J. Neurosci.* **32**, 10522–10529 (2012).
29. M. G. Heinz, E. D. Young, Response growth with sound level in auditory-nerve fibers after noise-induced hearing loss. *J. Neurophysiol.* **91**, 784–795 (2004).
30. E. F. Evans, The frequency response and other properties of single fibres in the guinea-pig cochlear nerve. *J. Physiol.* **226**, 263–287 (1972).
31. N. P. Cooper, W. S. Rhode, Nonlinear mechanics at the apex of the guinea-pig cochlea. *Hear. Res.* **82**, 225–243 (1995).
32. J. O. Pickles, Frequency threshold curves and simultaneous masking functions in high-threshold, broadly-tuned, fibres of the guinea pig auditory nerve. *Hear. Res.* **14**, 245–256 (1984).
33. A. R. Palmer, T. M. Shackleton, Variation in the phase of response to low-frequency pure tones in the guinea pig auditory nerve as functions of stimulus level and frequency. *J. Assoc. Res. Otolaryngol.* **10**, 233–250 (2008).
34. C. P. C. Versteegh, S. W. F. Meenderink, M. van der Heijden, Response characteristics in the apex of the gerbil cochlea studied through auditory nerve recordings. *J. Assoc. Res. Otolaryngol.* **12**, 301–316 (2011).
35. P. Dallos, M. C. Billone, J. D. Durrant, C. Wang, S. Raynor, Cochlear inner and outer hair cells: Functional differences. *Science* **177**, 356–358 (1972).
36. A. Fridberger, I. Tomo, M. Ulfendahl, J. Boutet de Monvel, Imaging hair cell transduction at the speed of sound: Dynamic behavior of mammalian stereocilia. *Proc. Natl. Acad. Sci. U.S.A.* **103**, 1918–1923 (2006).
37. P. Hakizimana, A. Fridberger, Inner hair cell stereocilia are embedded in the tectorial membrane. *Nat. Comm.* **12**, 2604 (2021).
38. A. J. Ricci, H. J. Kennedy, A. C. Crawford, R. Fettiplace, The transduction channel filter in auditory hair cells. *J. Neurosci.* **25**, 7831–7839 (2005).
39. L. Wagner, R. Altindal, S. K. Plontke, T. Rahne, Pure tone discrimination with cochlear implants and filter-band spread. *Sci. Rep.* **11**, 20236 (2021).
40. M. F. Dorman, T. Spahr, R. Gifford, L. Loiselle, S. McKarns, T. Holden, M. Skinner, C. Finley, An electric frequency-to-place map for a cochlear implant patient with hearing in the nonimplanted ear. *J. Assoc. Res. Otolaryngol.* **8**, 234–240 (2007).
41. A. R. Palmer, I. J. Russell, Phase-locking in the cochlear nerve of the guinea-pig and its relation to the receptor potential of inner hair-cells. *Hear. Res.* **24**, 1–15 (1986).
42. P. Jean, T. Anttonen, S. Michanski, A. M. G. de Diego, A. M. Steyer, A. Neef, D. Oestreicher, J. Kroll, C. Nardis, T. Pangršič, W. Möbius, J. Ashmore, C. Wichmann, T. Moser,

Macromolecular and electrical coupling between inner hair cells in the rodent cochlea. *Nat. Comm.* **11**, 3208 (2020).
43. R. K. Wang, A. L. Nuttall, Phase-sensitive optical coherence tomography imaging of the tissue motion within the organ of Corti at a subnanometer scale: A preliminary study. *J. Biomed. Opt.* **15**, 056005 (2010).

Acknowledgments: T. Ren and L. Reiss are acknowledged for comments, as well as J. Razzell Hollis for discussions on data visualization. **Funding:** This work was funded by U.S. National Institutes of Health grant R01-DC000141 (to A.L.N. and A.F.) and Swedish Research Council grants 2017-06092 and 2018-02692 (to A.F.). **Author contributions:** Conceptualization: G.B., A.F., and A.L.N. Methodology: A.F. and A.L.N. Formal analysis: A.F. and G.B. Investigation: G.B., P.H., A.F., and A.L.N. Visualization: A.F. and G.B. Funding acquisition: A.F. and A.L.N. Supervision: A.L.N. and A.F. Writing—original draft: A.F. Writing—review and editing: G.B., A.F., A.L.N., and P.H. **Competing interests:** The authors declare that they have no competing interests. **Data and materials availability:** The data needed to evaluate the conclusions in the paper can be downloaded at https://osf.io/teha9. All data needed to evaluate the conclusions in the paper are present in the paper and/or the Supplementary Materials.

Submitted 1 April 2022
Accepted 5 August 2022
Published 23 September 2022
10.1126/sciadv.abq2773